Materials Advances

ROYAL SOCIETY OF CHEMISTRY

PAPER

View Article Online
View Journal | View Issue

Check for updates

Cite this: *Mater. Adv.*, 2024, 5, 7401

Multi-stimuli-responsive behaviours of fluorenone-based donor–acceptor–donor triads in solution and supramolecular gel states†

Mao Suzuki,[a] Atsushi Seki,[ab] *[ab] Syota Yamada[a] and Ken'ichi Aoki[ab]

Received 7th May 2024,
Accepted 13th August 2024

DOI: 10.1039/d4ma00477a

rsc.li/materials-advances

Bilaterally asymmetric and symmetrical fluorenone-based donor–acceptor–donor (D–A–D) triads bearing hydrogen-bonded urethane units were synthesised in this study. Both the fluorenone derivatives exhibited supramolecular gelation in organic solvents. While the bilaterally asymmetrical fluorenone-based mono-urethane formed supramolecular gel in medium-chain linear alkanes and *n*-dodecyl benzene, the bilaterally symmetrical bis-urethane gelated to form *n*-dodecyl benzene and some mixed solvents. In the absorption spectra of these two compounds, two absorption peaks attributable to π–π* and intramolecular charge transfer (ICT) transitions were found. These D–A–D triads show emission from a twisted intramolecular charge transfer (TICT) state, together with photoluminescence from locally excited states. Solvatofluorochromic and acidifluorochromic behaviours were confirmed in dilute solutions for both compounds. While the fluorenone-based mono-urethane organogel displayed an acid-responsive colour change, the aromatic bis-urethane organogel changed its aggregation behaviour in response to trifluoroacetic acid. This study revealed that these D–A–D triads have the potential to be used as chemoresponsive materials for the multi-mode detection of target species.

Introduction

Environmentally responsive π-conjugated compounds are attractive materials for various applications such as security inks, sensors, smart windows, and smart devices, because they undergo spectral changes due to the structural variation under light, heat, humidity, or mechanical stimuli.[1–7] In particular, organic π-conjugated dyes bearing a donor–acceptor (D–A) framework have been extensively studied for their electro-optical and opto-electronic functions.[8–13] During intramolecular charge transfer (ICT) from electron-rich donor to electron-deficient acceptor units in D–A π-conjugated dyes there appears a characteristic light absorption and luminescence.[14,15] In addition, some D–A-type π-conjugated compounds exhibit favourable fluorescent properties *via* a twisted intramolecular charge transfer (TICT) state.[14–16] Because the ICT behaviour is sensitive to a polar environment, D–A type π-conjugated dyes could prove to be a useful material for the (fluoro)colorimetric detection of external stimuli.[15] In fact, mechanofluorochromic, electrochromic, thermochromic, solvatochromic, and acidochromic properties of D–A π-conjugated dyes have been reported.[17–20]

Supramolecular gels are fascinating soft matters that act as platforms for stimuli-responsive materials.[4,6,21–24] Thus, various organogelators composed of π-conjugated compounds, called "π-gelators", have been developed in the last few decades.[25–27] The synergistic effect of various intermolecular interactions leads to the formation of supramolecular gels composed of low-molecular-weight gelators (LMWGs) and appropriate solvents.[15,28,29] Therefore, supramolecular gels have the potential to translate molecular-scale information into bulk performance by tuning the balance of intermolecular interactions.[25,30,31] In this context, various supramolecular gelators which exhibit colour change and structural transformation to deal with external stimuli such as light and heat have been reported.[32–36] In addition to these physical stimuli-responsive LMWGs, supramolecular gel systems in response to chemical stimuli have also been developed.[37–43] For instance, Lehn and co-workers reported a guanosine derivative exhibiting ion-responsive LMWGs.[44] In typical ion response systems, the molecular-scale structural change driven by metal coordination, intercalation, or metal templating is amplified to macroscopic phase transition as well as spectral change.[39–44] A similar mechanism is adopted by functional LMWGs to respond to other chemical species. Based on the conventional

[a] *Department of Chemistry, Graduate School of Science, Tokyo University of Science, 1-3 Kagurazaka, Shinjuku-ku, Tokyo 162-8601, Japan. E-mail: a_seki_3@rs.tus.ac.jp*
[b] *Department of Chemistry, Faculty of Science, Tokyo University of Science, 1-3 Kagurazaka, Shinjuku-ku, Tokyo 162-8601, Japan*

† Electronic supplementary information (ESI) available. See DOI: https://doi.org/10.1039/d4ma00477a

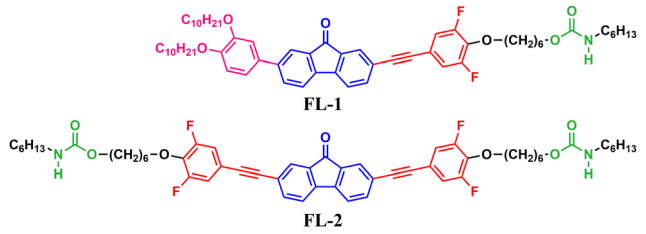

Fig. 1 Chemical structures of fluorenone-based D–A–D triads **FL-1** and **FL-2**.

molecular design of chemically stimuli-responsive LMWGs, the functional moiety that strongly interacts with the target species is attached to the fundamental unit to form supramolecular assemblies.[31]

Our present aim is to develop novel environmentally responsive ''π-gelators'' applicable to chemical indicators. Herein, we propose fluorenone-based donor–acceptor–donor (D–A–D) triads bearing hydrogen-bonded units as candidates for multi-stimuli-responsive bulk materials. Fluorenone is one of the attractive molecular skeletons acting as an electron acceptor with a planar π-conjugated system which shows high thermal stability. The rigid aromatic moiety is a promising building block for electron transport as well as stimuli-responsive photophysical switching and variation of self-assembling behaviours.[45–52] Thus, several fluorenone-based functional soft matters have been developed.[52–60] While various fluorenone-based D–A molecules working as fluorescent and colorimetric chemo-sensors in solution states have been reported,[49,61–68] a limited number of studies have reported multi-stimuli-responsive supramolecular gels of D–A-type fluorenone derivatives modified with alkoxybenzamide groups.[58] In this study, we expect that the cooperative intermolecular interactions of hydrogen bonding urethane units, fluorenone-based D–A–D aromatic core, and polar fluorine units are helpful to construct the multiple-sensing gel materials. Hence, D–A–D fluorenone-based monourethane **FL-1** and bisurethane **FL-2** were designed and synthesised (Fig. 1). First, we investigated the gelation ability of the fluorenone derivatives in organic solvents. We verified the impact of intermolecular hydrogen bonds through the urethane units on the formation of supramolecular self-assemblies. Furthermore, environmental stimuli-responsive behaviours were studied. The chromic behaviours based on π–π* and ICT transitions in solution and gel states as well as the transformation of aggregates in response to the acid were examined using **FL-1** and **FL-2**.

Experimental methods

General procedures

All ^{1}H and ^{13}C NMR spectra were recorded using a Bruker Biospin AVANCE NEO 400 spectrometer (400 MHz for ^{1}H NMR spectra and 100 MHz for ^{13}C NMR spectra). All chemical shifts (δ) in the ^{1}H and ^{13}C NMR spectra are quoted in ppm using tetramethylsilane (δ = 0.00 ppm) as the internal standard (0.03 vol%). High-resolution electrospray ionisation-mass spectrometry (HR-ESI-MS) was performed using a SCIEX X500R QTOF spectrometer.

Materials and synthesis

All the reagents were purchased from Tokyo Chemical Industry, Kanto Chemicals, and FUJIFILM Wako Pure Chemical Corporation. All the reagents were used without further purification. All the reactions were performed under an argon atmosphere in a well-dried three-necked flask equipped with a magnetic stirring bar.

Evaluation of gelation abilities and morphological study of xerogels

The samples were prepared as follows: an appropriate volume of organic solvent was added to 5 mg of the D–A–D-type fluorenone derivatives in 2 mL glass vials. The vials were sealed, and the samples were heated. When clear solutions were obtained upon heating, the mixture was cooled to room temperature. When a vial could be inverted without any flow, it was determined to be a 'gel'. In the cases where precipitation was observed during cooling, was termed as 'precipitation'. When the clear solutions, in contrast, remained after cooling, it was determined as 'soluble'. When the compound could not be dissolved completely even after it was sufficiently heated, it was determined to be 'insoluble'. The morphologies of the xerogel samples were investigated using scanning electron microscopy (SEM). The xerogel of **FL-1** was prepared from *n*-octane gel (20 g L^{-1}) by slow evaporation. The xerogel of **FL-2** was prepared from toluene/*n*-octane (1/1; mol/mol) gel (20 g L^{-1}) in a similar manner. Scanning electron microscopy (SEM) was performed under low-vacuum conditions using a JEOL JCM-6000 instrument.

Evaluation of phase transition behaviours

The thermal phase transition behaviour of pristine D–A–D-type fluorenone derivatives was characterised using polarising optical microscopy (POM) and differential scanning calorimetry (DSC). A polarising optical microscope (Olympus BH2) equipped with a digital camera (AS ONE HDCE-X1) and a temperature control system (Mettler Toledo FP90 and FP82HT) were used to visually observe the optical textures. For POM observation, indium tin oxide (ITO) sandwich cells filled with the samples π-conjugated compounds were used. Empty ITO sandwich cells (KSSO-02/A311P1NSS05, cell gap: 2 μm) were purchased from the EHC Corporation. The ITO surface without a polyimide was rubbed to facilitate planar orientation. DSC measurements were conducted using a SHIMADZU DSC-60 system equipped with a liquid nitrogen auto-cooling system (TAC-60L). For DSC measurements, approximately 2–3 mg of each sample was sealed in an aluminium pan.

FT-IR measurement of bulk and solution samples

FT-IR measurements were carried out on a Thermo Scientific Nicolet iS5 spectrometer in the transmission mode. For the variable-temperature FT-IR measurements, a handmade thermal control system composed of a silicone rubber heater, a

thermocouple sensor, and a PID-type thermal controller (AS ONE TJA-550) were used as additional equipment. For the measurements of the solution samples, a liquid sample cell composed of a silicone rubber spacer and a pair of KBr substrates were used. Bulk samples were prepared on Si substrates.

Characterization of spectroscopic properties in solution states

The UV-Vis absorption spectra in the solution state were recorded using a JASCO V-650 spectrometer. The UV-Vis absorption spectra of the dilute solutions were measured using a pair of quartz cells (cell path length: 1 cm). Photoluminescence emission spectra in the solution state were recorded using a SHIMADZU RF-6000 spectrometer. The emission spectra of the dilute solutions were recorded using a quartz cell (cell path length = 1 cm).

Characterization of the spectroscopic properties of bulk samples

Bulk samples were prepared on quartz substrates with a thickness of 1 mm. The UV-Vis absorption spectra of the bulk samples, except for the spectra of the samples treated with acid and base, were recorded using a JASCO V-650 spectrometer. The absorption spectra of the acid- and base-added samples were recorded using a Yixi Intelligent Technology YSM-8101-02-01-16S03L02F06G01 spectrometer equipped with a YLS-8301-01 deuterium halogen light source and quartz optical fibres. Photoluminescence spectra of the bulk samples were recorded using a Yixi Intelligent Technology YSM-8101-02-01-16S03L02F06G01 spectrometer. An LED light source (CCS HLV2-24UV3-365) with a control unit (CCS PJ2-1505-2CA-PE) was used for the photoexcitation.

Measurement of photoluminescence quantum efficiency and luminescence lifetime

The measurement of photoluminescence quantum yield (PLQY) was carried out on a Hamamatsu Photonics Quantaurus-QY. The emission decay profiles were recorded using a Hamamatsu Photonics Quantaurus-Tau. The PLQY and luminescence lifetime of the dilute solutions were measured using a quartz cell (cell path length = 1 cm). A quartz cell for solid-state samples was used for measuring the PLQY and luminescence lifetime of organogels. The PLQY of gel samples was determined from average of measurement values at the four different positions.

Evaluation of acid-responsive behaviours of organogels

An appropriate amount of trifluoroacetic acid (TFA) was added to the organogels. After the mixtures were heated above gel–sol transition temperature to be homogenized, the samples were left standing and gradually cooled down to room temperature. Then, the gelation abilities and spectroscopic properties were evaluated. The samples neutralized with triethylamine (TEA) were evaluated in the same way.

Results and discussion

Gelation behaviours of FL-1 and FL-2

The fluorenone derivatives **FL-1** and **FL-2** were synthesised as shown in Scheme S1 (see the ESI†). We examined the gelation properties of **FL-1** and **FL-2**, which are summarised in Table 1. These two fluorenone-based triads formed supramolecular gels in several solvents (Fig. 2a and b): **FL-1** and **FL-2** gelated dodecylbenzene (DB); however, the gelation behaviour of **FL-1** differed from that of **FL-2**. Compared to the gelation properties of these two compounds for DB, the minimum gel concentrations of bilaterally symmetrical bis-urethane **FL-2** were lower than those of mono-urethane **FL-1**. Thus, we concluded that **FL-2** was superior to **FL-1** in terms of the gelation ability of DB. As the gelation behaviours of the other solvents were studied, mono-urethane **FL-1** formed supramolecular organogels in medium-chain linear alkanes, such as *n*-octane, *n*-decane, and *n*-dodecane (Fig. 2a), whereas bis-urethane **FL-2** showed no gelation ability for those alkanes. Interestingly, the fluorenone-based triad **FL-2** formed supramolecular networks in a deep eutectic solvent (DES) comprised of *n*-decanoic acid/L-menthol (1/1; mol/mol) and equimolar mixed solvents with toluene and medium-chain linear alkanes (Fig. 2b). The gelation abilities of **FL-2** for toluene/*n*-octane (1/1; mol/mol) (T/O) and toluene/*n*-dodecane (1/1; mol/mol) (T/DD) are comparable. Because the solubilities of the aromatic solvents are quite different from **FL-1** and **FL-2**, mixtures of **FL-1** and these equimolar mixed solvents form weak gels.

POM and SEM observations were conducted to gain further insight into the morphology of the organogels. In the POM observation for organogels of **FL-1** in the open nicol arrangement, we observed ''sea anemone''-like aggregates in which many fibre bundles were entangled (Fig. S1 in the ESI†). We observed a contrasting optical texture in the POM for the organogels of **FL-2** in the open nicol arrangement (Fig. S2 in the ESI†).

Table 1 Gelation properties of **FL-1**, and **FL-2** at a concentration of 50 g L^{-1} (minimum gel concentrations given in g L^{-1})[a]

Solvent	FL-1	FL-2
n-Hexane	P	I
n-Octane	G (15)	P
n-Decane	G (11)	P
n-Dodecane	G (16)	P
Toluene	S	P
o-Xylene	S	P
m-Xylene	S	P
p-Xylene	S	P
Dodecylbenzene (DB)	G (33)	G (8)
Toluene/*n*-octane (1/1; mol/mol) (T/O)	WG	G (16)
Toluene/*n*-dodecane (1/1; mol/mol) (T/DD)	WG	G (13)
Chloroform	S	S
Ethyl acetate	P	GP
Acetone	P	GP
Methanol	P	GP
Deep eutectic solvent (DES)[b]	P	G (35)

[a] G, GP, I, S, P, and WG denote gel, gel-like precipitate, insoluble, soluble, precipitate, and weak gels, respectively. [b] *n*-Decanoic acid/L-menthol (1/1; mol/mol).

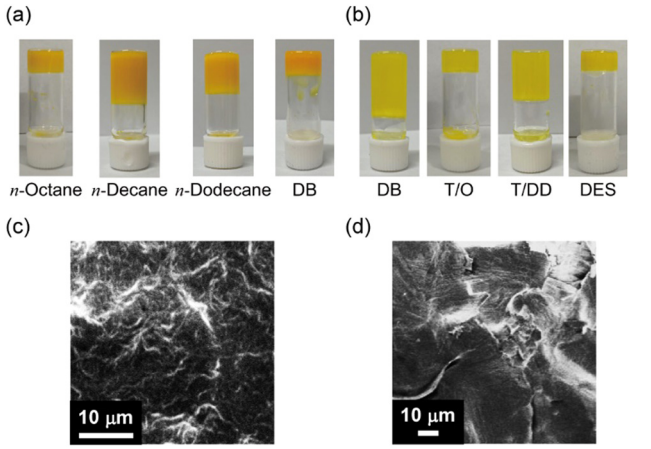

Fig. 2 (a) and (b) Photographs of organogels of (a) **FL-1** and (b) **FL-2** at minimum gel concentration in vials. (c) and (d) SEM images for xerogels of (c) **FL-1** and (d) **FL-2**.

The POM image indicated that sheet-like aggregates were formed in the oraganogel of **FL-2**. SEM observations of the xerogels also supported such a difference in gel morphologies between the organogels of **FL-1** and **FL-2** (Fig. 2c and d). In the SEM image of the xerogel prepared from *n*-octane gel of **FL-1**, flaccid fibrous aggregates with an average diameter of the submicron order were observed (Fig. 2c). In contrast, relatively high-straightness, elongated, and sheet-like objects were observed in the xerogel sample procured from the T/O gel of **FL-2** (Fig. 2d). The difference in these gelation and dissolution behaviours reflects the discrepancy in the self-assembled structures and the association process in supramolecular gels between **FL-1** and **FL-2**.

Self-assembling behaviours

FT-IR spectra provide valuable information about the intermolecular hydrogen bonding modes among the urethane units. First, the self-assembly behaviour of the fluorenone derivatives was examined in detail. In the pristine crystalline phase of **FL-1**, the peaks of N–H and C=O stretching vibration were observed at 3323 cm^{-1} and 1683 cm^{-1}, respectively (Fig. 3a, red line). These peaks indicated that molecules of **FL-1** formed intermolecular hydrogen bond networks in the room-temperature crystalline phase.[69–71] Similarly, the FT-IR spectrum in the crystalline phase of **FL-2** involved the broad hydrogen-bonded N–H vibration peak at 3332 cm^{-1} and sharp hydrogen-bonded C=O vibration signal at 1687 cm^{-1} (Fig. 3b, red line). In contrast, the signals around 3330 and 1685 cm^{-1} became ambiguous in the FT-IR spectra of the THF solutions of **FL-1** and **FL-2** (Fig. 3a and b; black lines). These results suggest the existence of intermolecular hydrogen bond networks among the urethane units in the crystalline state. The formation of the intermolecular hydrogen bond was additionally corroborated by the ^{1}H NMR spectra of **FL-1** and **FL-2** in DMSO-d_6/$CDCl_3$ (5/1; v/v). In their ^{1}H NMR spectra, a broad peak originating from the hydrogen-bonded N–H was found at δ = 9.51 ppm (Fig. S8, ESI†).[72]

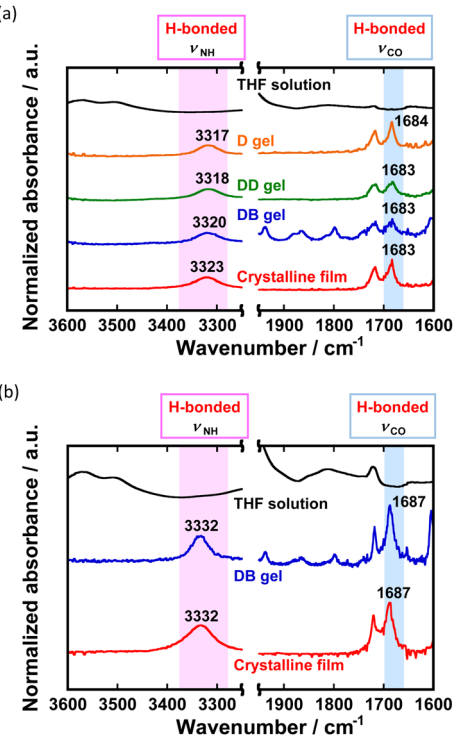

Fig. 3 FT-IR spectra of (a) **FL-1** and (b) **FL-2** in the THF solution, gel, and crystalline states.

XRD measurements were conducted on the pristine D–A–D triads to gain further insights into their crystalline structures. The complicated XRD pattern of the Cr_2 phase of **FL-1** (Fig. S6a, ESI†) was different from the diffraction pattern of a simple layered structure and is similar to the pattern of a cylindrical structure. The large layer spacing owing to the long molecular length (> 52 Å) of **FL-1** prevented us further structural analysis. Considering the molecular packing of aromatic compounds with similar shapes,[73–75] we assumed a possible molecular packing (Fig. S7a, ESI†) that resulted in the bundled fibrous aggregates. In contrast, the XRD study of **FL-2** revealed that the symmetrical bisurethanes formed a layered structure in the crystalline phases (Fig. S6b and S7b, ESI†). These considerations coincided with the results of the POM and SEM studies of the gels of **FL-1** and **FL-2**.

The thermal phase transition behaviours of the pristine compounds **FL-1** and **FL-2** are summarised in Table 2, and a detailed characterisation of the mesomorphic properties is shown in the ESI† (Fig. S3–S6). Interestingly, the bilaterally symmetrical bis-urethane **FL-2** exhibited two smectic liquid-crystalline phases.

Table 2 Phase transition behaviours of compounds **FL-1** and **FL-2**

Sample	Phase-transition temperature[a]/°C (enthalpy/kJ mol^{-1})
FL-1	Cr_2 93 (3) Cr_1 103 (51) IL
FL-2	Cr_1 6 (5) Cr_2 144 (15) M 150 (27) S_C 165 (1) S_A 177 (2) IL

[a] The abbreviations Cr, IL, S_A and S_C denote crystalline, isotropic liquid, smectic A, and smectic C phases, respectively, where M denotes an unidentified mesophase.

We performed variable temperature (VT)-FT-IR measurements to clarify the association–dissociation behaviours of the intermolecular hydrogen bond networks through thermal phase transition. In the VT-FT-IR spectrum of **FL-1** in the liquid phase at 126 °C, N–H and C═O vibration signals of intermolecular hydrogen-bonding were suppressed (Fig. S9a in the ESI†). The spectra indicated that the intermolecular hydrogen bonds were disordered and almost dissociated in the liquid state. The change in the VT-FT-IR spectra of **FL-2** suggested that bisurethane underwent a stepwise dissociation of intermolecular hydrogen bonds *via* several phase transitions (Fig. S9b in the ESI†).

Next, we examined the self-assembly behaviour of **FL-1** and **FL-2** in the gel state. The DB gels of **FL-1** and **FL-2** gave the similar spectral patterns to the FT-IR spectra of their crystalline solids (Fig. 3a and b; blue lines). The broad N–H signal around 3320–3335 cm^{-1} and sharp C═O signal around 1717–1720 cm^{-1} clearly suggested the existence of intermolecular hydrogen bond networks in the DB gel states. These results support the formation of intermolecular hydrogen-bonded arrays between urethane units to form supramolecular gels. It is noteworthy that the N–H band in DB gel of **FL-2** shifted 13 cm^{-1} to the higher wavenumber compared with that of **FL-1**. These results indicate that bisurethane **FL-2** forms weaker intermolecular hydrogen bonds between the urethane units than mono-urethane **FL-1**. Because the FT-IR spectra of **FL-2** in the gel state showed unimodal-shaped N–H and C═O vibration peaks, both urethane units in **FL-2** were probably in the same environment. Therefore, we consider that molecules of **FL-2** in the gel state are bound to adjacent molecules through equivalent intermolecular hydrogen bond networks at the two urethane units. Because polar structures are thermodynamically unfavourable in general, the relative positional relationship of the central ketone unit in the fluorenone core must be in a slip-stacked or anti-parallel H-stacked arrangement to minimize polarization in the aggregated structure. In addition, the curved molecular shape of **FL-2** should affect the average distance between adjacent urethane units owing to steric effects. As a result, the intermolecular hydrogen bonds in the gel states of **FL-2** were weaker than those in the gels of mono-urethane **FL-1**, owing to the balance of the intermolecular interactions between neighbouring molecules.

We investigated the influence of π–π interaction between the central aromatic cores upon self-assembling behaviours by UV-vis spectroscopy. The absorption spectra in toluene solutions, DB gels and crystalline films of **FL-1** and **FL-2** are shown in Fig. 4a and b. Both absorption spectra of **FL-1** and **FL-2** in toluene solution (10 μM) showed two strong absorption peaks with broad quasi-unimodal absorption band around 440 nm. While the absorptions at around 300 nm and 350 nm correspond to π–π* transition of central aromatic core, the broad absorption band is probably derived from ICT transition. This interpretation was supported by the simulation results of HOMO and LUMO distributions for **FL-1** and **FL-2** by density functional theory (DFT) calculations at the B3LYP/6-31G(d,p) level.[76–80] While the HOMOs of the fluorenone-based triads were delocalized over the central π-conjugated core, the LUMOs

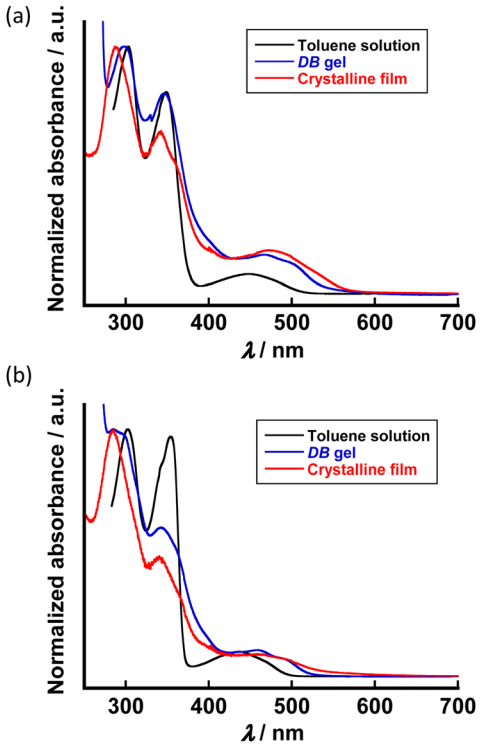

Fig. 4 UV-Vis spectra of (a) **FL-1** and (b) **FL-2** in the toluene solution (10 μM), dodecylbenzene gel and crystalline film states.

were localized on fluorenone unit (Fig. S10 in the ESI†). The difference in orbital spreading between HOMO and LUMO could be favourable for ICT. In the case of **FL-1**, the π–π* transition band in the absorption spectrum of the crystalline film was blue-shifted against the π–π* band in the absorption spectrum of toluene solution (10 μM). Although the bathochromic effect of π–π* transition band was also found in the DB gel to referenced spectrum of the dilute solution, the shift value of the DB gel was slightly smaller than that of the crystalline film. Despite the slight difference in the absorption spectra between the crystalline film and DB gel, the bathochromic shift of π–π* transition band indicated the formation of H-aggregate triggered by π–π interaction in the crystalline phase and DB gel state of **FL-1** (Fig. 4a and Table S2 in ESI†). As we consider the difference in shift between the DB gel and crystalline films, π–π interaction should be weakened in the DB gel than in the crystalline films for **FL-1**. It is noted that the similar trend was found in the other organogels of **FL-1** (Fig. S11a in the ESI†). The organogels of **FL-2** exhibited the analogous bathochromic effect of π–π* band to that of the crystalline films (Fig. 4b; Table S2 and Fig. S11b in the ESI†). Because the shift values of the highest peak for DB gel of **FL-2** were comparable to those for the crystalline film, a strong π–π interaction network between the central aromatic core was formed in the DB gel state as well as the crystalline state. The small gaps contributing to π–π interaction in self-assembling behaviour between **FL-1** and **FL-2** seemed to become apparent as variations of the

bathochromic effect and gel morphology (Fig. 2c and d). To summarise the results thus far, the supramolecular networks in the organogel of **FL-2** were probably stabilised in a cooperative manner by the multiple intermolecular interactions including hydrogen bonds at two sites and π–π interactions; thus, **FL-2** is considered to show more excellent gelation ability in DB than **FL-1**. Because the multi-point intermolecular hydrogen bond network between polar urethane units promotes the aggregation, the bisurethane **FL-2** did not exhibit gelation ability to non-polar hydrocarbon solvents.

Solvent-responsive behaviours in solution states

The absorption spectra of compounds **FL-1** and **FL-2** in solutions diluted by various solvents (10 μM) are shown in Fig. 5a and d. Because these two fluorenone derivatives showed low solubility to *n*-hexane, ethanol, and acetonitrile, we evaluated the spectroscopic properties for those by the mixed solvent system with chloroform. The absorption maxima and molar extinction coefficients in solutions of compounds **FL-1** and **FL-2** are summarised in Table S1 in the ESI.† Although we recognised small disparities between the absorption spectra of **FL-1** in each solvent (Fig. 5a), a slightly large difference in the molar extinction coefficient was found between the absorption spectra of **FL-2** in the various solvents (Fig. 5d). In addition, **FL-2** exhibited larger molar extinction coefficient than **FL-1**. These gaps were probably caused by the change in planarity of the D–A–D core in the solvation environment. In common to **FL-1** and **FL-2**, however, the solvatochromic behaviours based on the absorption properties were not conspicuous in solution states.

Because some D–A type π-conjugated compounds exhibit favourable photo-luminescent (PL) properties based on TICT, the emission properties of dilute solutions in various solvents (10 μM) were investigated. The absorption and emission maxima of various solutions of **FL-1** and **FL-2** are summarised in Table S1 in the ESI.† Compared to the absorption properties in the solution state of **FL-1** and **FL-2**, significant differences in the PL properties were observed. The emission colour in the solution state of these two compounds depended on the solvent species (Fig. 5b and e). In the solutions of **FL-1** diluted by nonpolar solvents such as toluene, ethyl acetate (EtOAc), THF and chloroform, a relatively strong TICT emission than the π–π* emission was observed (Fig. 5b). Considering the PL spectra of **FL-1** in DMF, acetonitrile/chloroform (1/9, v/v) ($CH_3CN/CHCl_3$), and ethanol/chloroform (1/9; v/v) (EtOH/$CHCl_3$) (Fig. 5b), TICT emission was suppressed in a highly polar environment. The emission maximum also shifted in response to the polar environment of the solution. In the case of **FL-2**, we observed a dull suppression of TICT emission in a highly polar atmosphere (Fig. 5e). Although the shift in the emission maxima in solutions of **FL-2** was slightly different from that in solutions of **FL-1**, both fluorenone-based D–A–D triads exhibited solvatofluorochromic behaviour in solution. The differences in the PL behaviours of **FL-1** and **FL-2** in the solution state could be visually discerned, as shown in Fig. 5c and f. In the solutions containing chloroform, the TICT emission band was significantly red-shifted than the other solvents showing less hydrogen bond donor ability (α).[81–85] This consideration was properly supported by Lippert–Mataga plots of **FL-1** and **FL-2**. The correlation between Stokes shift and orientational polarization (Δf) followed separated trends in the solutions involving chloroform and the others (Fig. S12, ESI†).[81–85] The Stokes shift roughly showed increasing trend as the polarity of the solvent increased. The low coefficient of determination (R^2) in the Lippert–Mataga plot of **FL-2** was

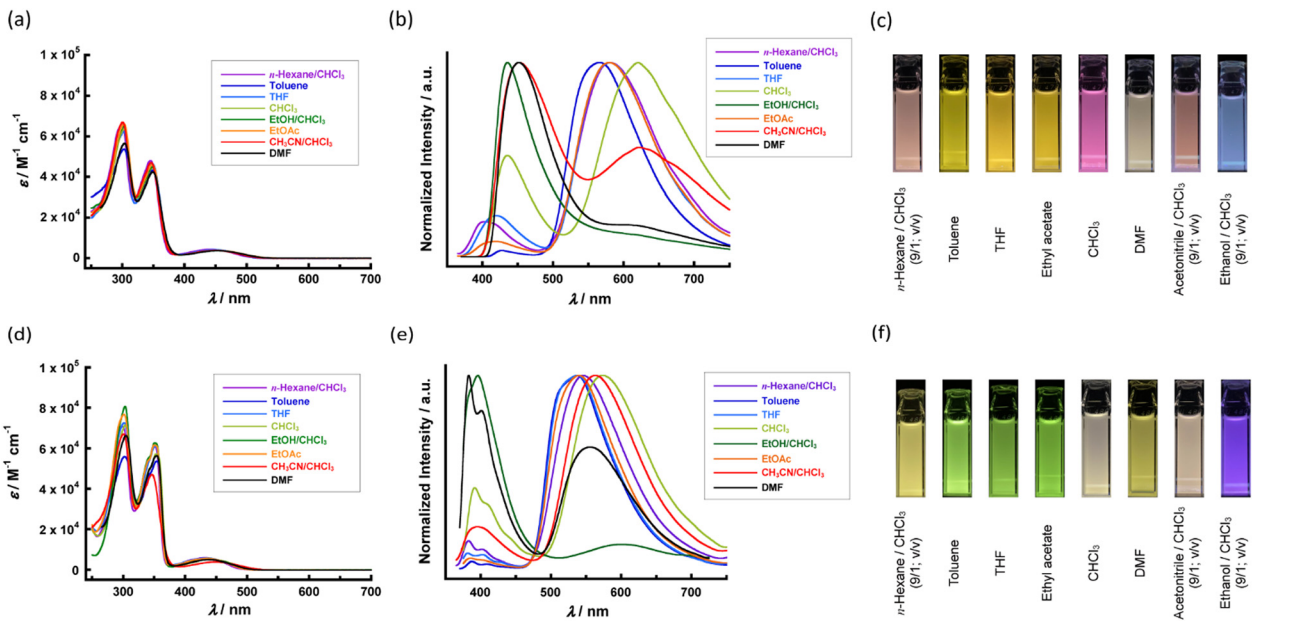

Fig. 5 (a) and (d) UV-Vis spectra of (a) **FL-1** and (d) **FL-2** in solutions diluted by the various solvents (10 μM). (b) and (e) PL spectra of (b) **FL-1** and (e) **FL-2** in solutions diluted by various solvents (10 μM). (c) and (f) Photographs for various solutions (10 μM) of (c) **FL-1** and (f) **FL-2** in vials under the UV-light (355 nm) irradiation.

probably caused by the contribution of α for EtOH as in the case of chloroform. The PL quantum yield (PLQY) was also evaluated of **FL-1** and **FL-2** in series of dilute solutions (Table S1, ESI†). Common to both compounds, the PLQY was lowered in polar media or chloroform-containing solutions owing to the quenching of TICT emission while high PLQY was confirmed in solutions diluted by non-polar solvents except for chloroform. Especially, the significant decrease of PLQY in the solutions including chloroform may be affected by the character of chloroform as a non-polar solvent but exhibiting hydrogen bond donor ability.[81–85] At the same time, luminescence can be easily identified even in polar solutions of **FL-2** because the fluorenone derivative **FL-2** exhibited higher PLQY than **FL-1** in almost all solvent systems (Fig. 5f and Table S1, ESI†). The difference in the solvatofluorochromic behaviour between the two compounds suggests a difference in the solvation behaviour of **FL-1** and **FL-2**. Although monourethane **FL-1** has two long aliphatic side chains on one wing and a polar hydrogen-bonding unit on the opposite wing, bisurethane **FL-2** has polar hydrogen-bonding units on both wings. This discrepancy in chemical structures should cause easily imaginable variations in intermolecular interactions between the molecules of the D–A–D triad and solvent molecules. Because the ICT state is a polar environment, solvent polarity affects the ICT-based photophysical properties through polar interactions. Thus, variations in self-absorption by the ICT absorption bands and quenching of ICT emissions should reflect the unique solvatofluorochromic behaviours of **FL-1** and **FL-2**. The PL lifetime at emission peaks was measured for various solutions of **FL-1** and **FL-2** to obtain further insights of the luminescence (Table S3, Fig. S13 and S14 in the ESI†). All fluorescence decay curves can be fitted with single exponential or biexponential curves. The photoluminescence at emission maxima around 400 nm in solutions of those two compounds exhibited fast decay with shorter lifetimes less than a few nano-seconds. Although the fluorescence lifetime of the longer-wavelength emission was long in non-polar solvents for each of the fluorenone derivatives, the solvation in polar medias shortened the lifetime of red-coloured emissions. The trends of varying the PLQY and lifetime of TICT emission correlates with the Stokes shifts. These results corroborated the solvatofluorochromic behaviour based on TICT in the fluorenone-based D–A–D triads.

Acid-responsive behaviours in solution states

The absorption spectra of dilute solutions (10 μM) after the addition of TFA are shown in Fig. 6a and d. When TFA of more than 10^4 eq. was added to the solution of **FL-1**, the absorption spectra changed slightly compared to the initial spectrum. Although the addition of an excessive amount of TFA enhanced the absorption peak of the high-energy transition, the ICT band broadened and redshifted (Fig. 6a). A similar TFA-responsive spectral change was also found in the case of **FL-2** (Fig. 6d). The PL spectra of dilute solutions (10 μM) with optional amounts of TFA are shown in Fig. 6b and e. Both D–A–D type fluorenone-based urethane compounds **FL-1** and **FL-2** exhibited drastic and noticeable PL emission spectral changes in response to the TFA. When an excess TFA of more than 10^5 eq. was added to each solution, the PL emission was quenched (Fig. 6b, c, e and f). The total quantum efficiency of the solution after the addition of TFA decreased by more than an order of magnitude (Table S3 in the ESI†). The response behaviours to TFA in the fluorescent properties were clearer than those in the absorption properties. The study of ^{13}C NMR suggested that the variations in the absorption and PL spectra were derived from the approach of

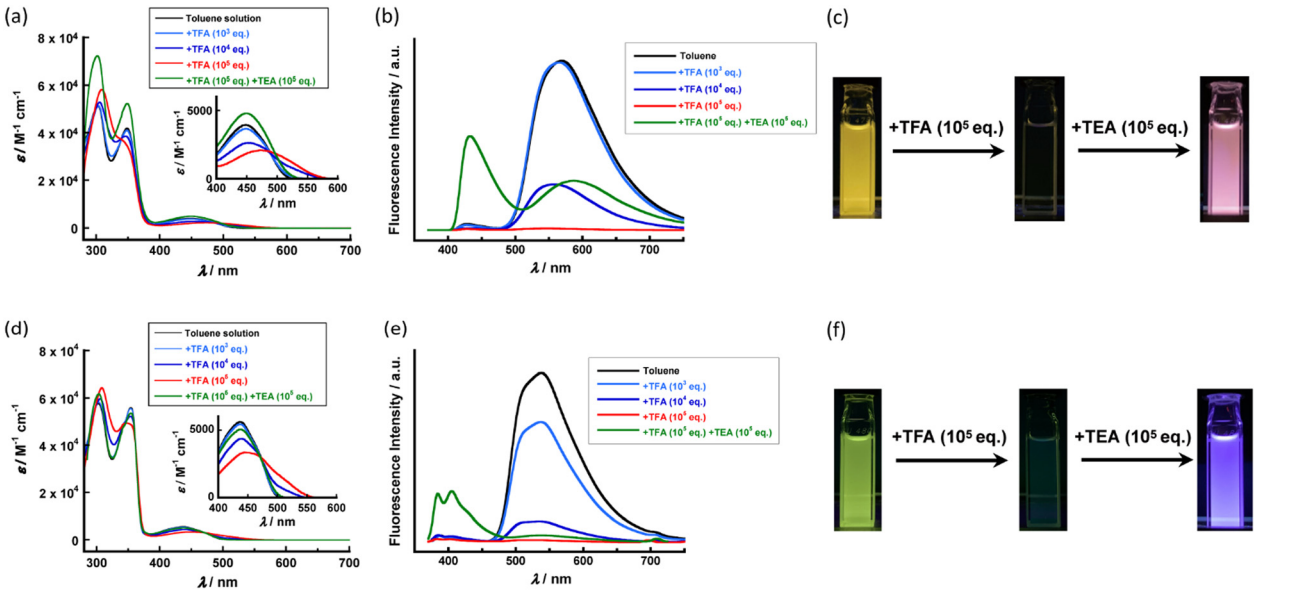

Fig. 6 (a), (b), (d) and (e) Changes of the spectroscopic properties in the THF solution (10 μM) in the TFA and subsequent TEA additions. (a) and (d) UV-Vis spectra of (a) **FL-1** and (d) **FL-2**. (b) and (e) PL spectra of (b) **FL-1** and (e) **FL-2**. (c) and (f) Photographs for the THF solution (10 μM) of (c) **FL-1** and (f) **FL-2** in the series of treatments in vials under the UV-light (355 nm) irradiation.

protons to the central ketone unit of the fluorenone core (Fig. S15 in the ESI†). After TFA was added to the sample solution of **FL-1**, the signal of the central ketone unit at δ = 193.1 ppm disappeared (Fig. S15a in the ESI†). The other signals of the aromatic carbon were also slightly shifted owing to the change in the electronic shielding environment. For **FL-2**, the signal at δ = 191.9 ppm also vanished (Fig. S15b in the ESI†). As the following addition of TEA resulted in further change of fluorescent properties, no recovery of the initial fluorescence colour was found in both cases. The addition of TEA to the acidified solutions increased the PLQY. However, the PLQY was not recovered to the original levels of the initial solutions before the addition of TFA (Table S4, ESI†). This is probably due to the difference in the environment of the fluorophore in the neutralized solution. The polar interaction between the fluorenone core and neutralized ionic species in the solution presumably affected the intramolecular motions of the D–A–D compound to suppress the TICT emission.

Acid-responsive behaviours in organogels

The TFA-responsive changes in the absorption of **FL-1** by organogels are shown in Fig. 7a. When the D gel of **FL-1** was treated by 1 eq. of TFA, the relative absorbance of ICT band became conspicuous against the initial absorption spectrum. The colour of the D gel changed from orange to reddish-orange upon the addition of acid (Fig. 7c). The addition of TFA also affected the emission properties of **FL-1** in D gel (Fig. 7b). The slightly red-shifted PL spectrum for the acidified gel of **FL-1** was probably affected by the self-absorption of the ICT absorption band. This consideration was also indicated by the decrease of PLQY by the addition of TFA (Table S5 in the ESI†). Since the variation of fluorescence lifetime (Table S5 and Fig. S16a in the ESI†) suggested the change of environment surrounding fluorophore in the supramolecular gel of **FL-1**, the interaction between the proton and carbonyl unit of the fluorenone core should have caused a colour change similar to that in the solution system (Fig. S17a in the ESI†). Subsequent addition of TEA suppressed the ICT absorbance. When the gel of **FL-1** recovered orange colour (Fig. 7a and c), the PLQY and fluorescence lifetime were also almost fully restored (Table S5 and Fig. S16a, ESI†). Even after a series of acid and base treatments, the gel state was retained by the mixture of **FL-1** and solvent. The absorption spectra of the initial DB gel of **FL-2** and samples with additives are shown in Fig. 7d. Although the TFA-responsive colour change was evident in the D gel of **FL-1**, the mixed sample of **FL-2** exhibited a gentle spectral change in response to TFA (Fig. 7d–f). While the acidification by TFA distinctively reduced the PLQY in the D gel system of **FL-1**, the PLQY for the DB gel of **FL-2** was slightly increased after addition of the acidic species (Table S5, ESI†). Although the DB gel of **FL-2** showed ambiguous responsivity in the absorption colour to TFA, the aggregation behaviour changed significantly. When TFA (1.0 eq.) was added to the DB gel of **FL-2**, the gel collapsed (Fig. 7f). The slight changes in PLQY and emission lifetime may have stemmed from crumbling of the supramolecular gel (Table S5 and Fig. S16b, ESI†). Because the protons derived from TFA could access the polar urethane units and the central carbonyl group of the fluorenone core, the disintegration of the supramolecular gel was probably caused by disordered intermolecular hydrogen bonding. As previously discussed, the DB gel of **FL-2** is considered to possess weakened hydrogen bonds. Therefore, it is more likely that the protonation of the urethane units has a fatal influence on the hydrogen bonding networks in the **FL-2** gel sufficient to disrupt the self-assembled

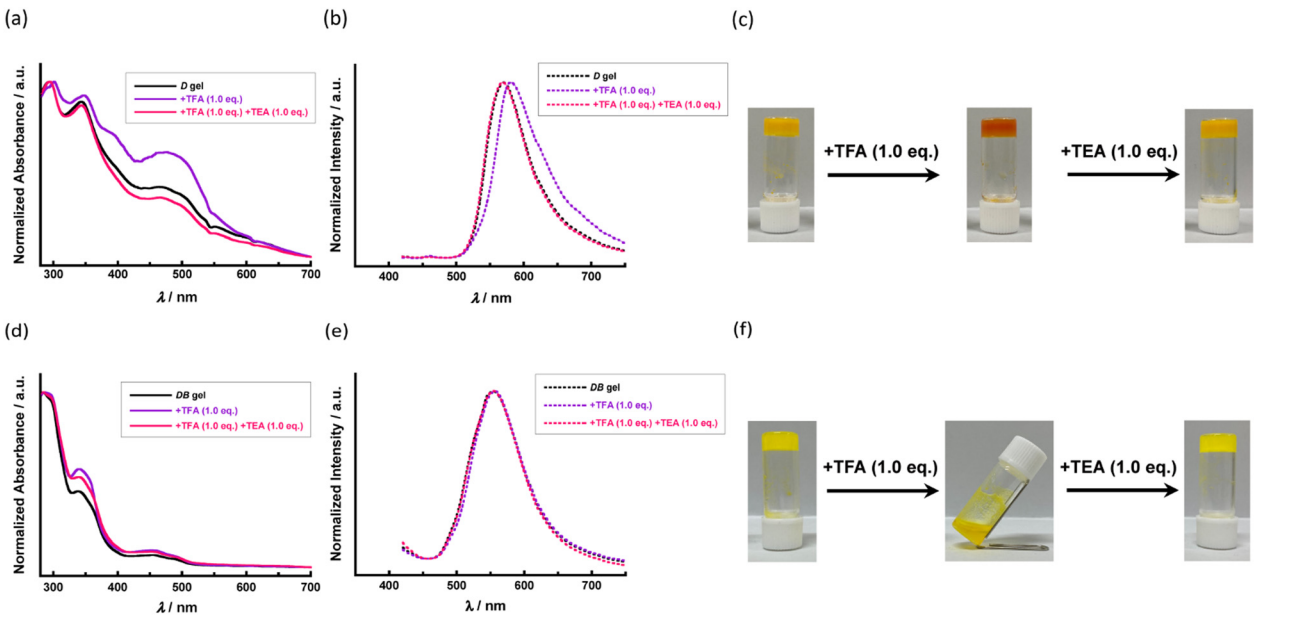

Fig. 7 (a), (b), (d) and (e) Changes of the spectroscopic properties in the gel states after the addition of TFA and subsequent TEA treatment. (a) and (d) UV-Vis spectra for (a) D gel of **FL-1** and (d) DB gel of **FL-2**. (b) and (e) PL spectra for (b) D gel of **FL-1** and (e) DB gel of **FL-2**. (c) and (f) The appearance changes in the gel states after the series of treatments. Photographs for (c) D gel of **FL-1** and (f) DB gel of **FL-2** in vials under the ambient light.

structures (Fig. S17b in the ESI†). Because the dense environment in the gel states should be favourable for the association of protons and fluorenone derivatives compared to the solution states, the sensitivity to TFA in the gel states was several orders of magnitude higher than that in the dilute solutions state. Neutralisation of the acidified sample with 1.0 eq. of TEA led to the reformation of an organogel (Fig. 7f), so that the PLQY and fluorescence lifetime were recovered (Table S5 and Fig. S16b, ESI†). Although clear TFA-responsive absorption and PL spectral changes were observed for the D gel of monourethane **FL-1**, transformation of supramolecular aggregates in response to TFA was confirmed for the DB gel of bisurethane **FL-2**. Each of the fluorenone derivatives **FL-1** and **FL-2** showed different TFA-responsive behaviours in the organogel states.

Conclusions

In this study, bilaterally asymmetrical and symmetrical liquid-crystalline fluorenone derivatives bearing urethane units were synthesised. These two compounds formed supramolecular gels in the appropriate solvents. The spectroscopic study suggested that the driving force of the gelation is intermolecular hydrogen bonding and π–π interaction between the adjacent dye molecules. Both D–A–D triads exhibited ICT, which became visible in the absorption and PL bands. The solvent-dependent emission colour change and TFA-responsive chromic behaviour were found in the solutions. In addition, the organogels exhibited TFA-responsive colour or agglomeration changes. Fluorenone-based D–A–D triads have the potential to pave the way for a material system that is applicable for the multi-mode detection of several chemical stimuli.

Author contributions

Conceptualisation, A. S.; data curation, M. S., S. Y., A. S. and K. A.; formal analysis, M. S. and A. S.; funding acquisition, A. S. and K. A.; investigation, M. S., S. Y. and A. S.; methodology, A. S.; project administration, A. S.; resources, A. S. and K. A.; supervision, A. S. and K. A.; validation, M. S. and A. S.; visualisation, M. S. and A. S.; writing – original draft, A. S.; writing – review and editing, M. S., A. S., S. Y. and K. A. All authors have read and agreed to the published version of the manuscript.

Data availability

The data supporting this article have been included as part of the ESI.†

Conflicts of interest

The authors declare no conflicts of interest.

Acknowledgements

The authors thank Prof. Dr N. Nakamura and Prof. Dr T. Ichikawa at the Tokyo University of Agriculture and Technology for their help with the SEM observations. The authors are grateful to Prof. Dr Y. Sagara and Mr S. Shimizu at Tokyo Institute of Technology for assistance with the measurements of PLQY, emission lifetime, and the photoluminescence emission spectra in the bulk state. The authors also greatly appreciate the help of Dr Y. Yoshimura at Tokyo University of Science with the HRMS measurements. This study was financially supported by research funds from the Tokyo University of Science for A. S. and K. A. This study was also financially supported by Research Grant from the JKA (2023-No. 337) for A. S.

References

1 S. W. Thomas, G. D. Joly and T. M. Swager, Chemical Sensors Based on Amplifying Fluorescent Conjugated Polymers, *Chem. Rev.*, 2007, **107**, 1339–1386.
2 B. Yoon, D.-Y. Ham, O. Yarimaga, H. An, C. W. Lee and J.-M. Kim, Inkjet Printing of Conjugated Polymer Precursors on Paper Substrates for Colorimetric Sensing and Flexible Electrothermochromic Display, *Adv. Mater.*, 2011, **23**, 5492–5497.
3 V. K. Praveen, B. Vedhanarayanan, A. Mal, R. K. Mishra and A. Ajayaghosh, Self-Assembled Extended π-Systems for Sensing and Security Applications, *Acc. Chem. Res.*, 2020, **53**, 496–507.
4 F. J. M. Hoeben, P. Jonkheijm, E. W. Meijer and A. P. H. J. Schenning, About Supramolecular Assemblies of π-Conjugated Systems, *Chem. Rev.*, 2005, **105**, 1491–1546.
5 Y. Sagara, S. Yamane, M. Mitani, C. Weder and T. Kato, Mechanoresponsive Luminescent Molecular Assemblies: An Emerging Class of Materials, *Adv. Mater.*, 2016, **28**, 1073–1095.
6 N. M. Sangeetha and U. Maitra, Supramolecular gels: Functions and uses, *Chem. Soc. Rev.*, 2005, **34**, 821–836.
7 C. D. Jones and J. W. Steed, Gels with sense: supramolecular materials that respond to heat, light and sound, *Chem. Soc. Rev.*, 2016, **45**, 6546–6596.
8 A. Mishra, M. K. R. Fischer and P. Bäuerle, Metal-Free Organic Dyes for Dye-Sensitized Solar Cells: From Structure: Property Relationships to Design Rules, *Angew. Chem., Int. Ed.*, 2009, **48**, 2474–2499.
9 Y. Lin, Y. Li and X. Zhan, Small molecule semiconductors for high-efficiency organic photovoltaics, *Chem. Soc. Rev.*, 2012, **41**, 4245–4272.
10 Y. Wu and W. Zhu, Organic sensitizers from D–π–A to D–A–π–A: effect of the internal electron-withdrawing units on molecular absorption, energy levels and photovoltaic performances, *Chem. Soc. Rev.*, 2013, **42**, 2039–2058.
11 S. Barlow and S. R. Marder, Nonlinear Optical Properties of Organic Materials, in *Functional Organic Materials*, ed. T. J. J.

Müller and U. H. F. Bunz, Wiley-VCH, Weinheim, Germany, 2007, pp. 393–437.
12 M. Szablewski, P. R. Thomas, A. Thornton, D. Bloor, G. H. Cross, J. M. Cole, J. A. K. Howard, M. Malagoli, F. Meyers, J.-L. Brédas, W. Wenseleers and E. Goovaerts, Highly Dipolar, Optically Nonlinear Adducts of Tetracyano-*p*-quinodimethane: Synthesis, Physical Characterization, and Theoretical Aspects, *J. Am. Chem. Soc.*, 1997, **119**, 3144–3154.
13 R. R. Tykwinski, U. Gubler, R. E. Martin, F. Diederich, C. Bosshard and P. Günter, Structure–Property Relationships in Third-Order Nonlinear Optical Chromophores, *J. Phys. Chem. B*, 1998, **102**, 4451–4465.
14 Z. R. Grabowski, K. Rotkiewicz and W. Rettig, Structural Changes Accompanying Intramolecular Electron Transfer: Focus on Twisted Intramolecular Charge-Transfer States and Structures, *Chem. Rev.*, 2003, **103**, 3899–4032.
15 Y. Li, T. Liu, H. Liu, M.-Z. Tian and Y. Li, Self-Assembly of Intramolecular Charge-Transfer Compounds into Functional Molecular Systems, *Acc. Chem. Res.*, 2014, **47**, 1186–1198.
16 S. Sasaki, G. P. C. Drummen and G. Konishi, Recent advances in twisted intramolecular charge transfer (TICT) fluorescence and related phenomena in materials chemistry, *J. Mater. Chem. C*, 2016, **4**, 2731–2743.
17 X. Y. Shen, Y. J. Wang, E. Zhao, W. Z. Yuan, Y. Liu, P. Lu, A. Qin, Y. Ma, J. Z. Sun and B. Z. Tang, Effects of Substitution with Donor–Acceptor Groups on the Properties of Tetraphenylethene Trimer: Aggregation-Induced Emission, Solvatochromism, and Mechanochromism, *J. Phys. Chem. C*, 2013, **117**, 7334–7347.
18 J. Sun, X. Lv, P. Wang, Y. Zhang, Y. Dai, Q. Wu, M. Ouyang and C. Zhang, A donor–acceptor cruciform π-system: high contrast mechanochromic properties and multicolour electrochromic behavior, *J. Mater. Chem. C*, 2014, **2**, 5365–5371.
19 J. Tong, Y. Wang, J. Mei, J. Wang, A. Qin, J. Z. Sun and B. Z. Tang, A 1,3-Indandione-Functionalized Tetraphenylethene: Aggregation-Induced Emission, Solvatochromism, Mechanochromism, and Potential Application as a Multiresponsive Fluorescent Probe, *Chem. – Eur. J.*, 2014, **20**, 4661–4670.
20 C. Dou, L. Han, S. Zhao, H. Zhang and Y. Wang, Multi-Stimuli-Responsive Fluorescence Switching of a Donor–Acceptor π-Conjugated Compound, *J. Phys. Chem. Lett.*, 2011, **2**, 666–670.
21 T. Ishi-I and S. Shinkai, Dye-Based Organogels: Stimuli-Responsive Soft Materials Based on One-Dimensional Self-Assembling Aromatic Dyes, *Top. Curr. Chem.*, 2005, **258**, 119–160.
22 X. Du, J. Zhou, J. Shi and B. Xu, Supramolecular Hydrogelators and Hydrogels: From Soft Matter to Molecular Biomaterials, *Chem. Rev.*, 2015, **115**, 13165–13307.
23 D. Han, J. Wang, T. Zheng, L. Peng and T. Jiao, Supramolecular assembly with stimuli-responsive circularly polarized luminescence, *Cell Rep. Phys. Sci.*, 2023, **4**, 101523.
24 S. He, Z. Jiang, X. Dou, L. Gao and C. Feng, Chiral Supramolecular Assemblies: Controllable Construction and Biological Activity, *ChemPlusChem*, 2023, **88**, e202300226.
25 Z. Qi and C. A. Schalley, Exploring Macrocycles in Functional Supramolecular Gels: From Stimuli Responsiveness to Systems Chemistry, *Acc. Chem. Res.*, 2014, **47**, 2222–2233.
26 S. S. Babu, V. K. Praveen and A. Ajayaghosh, Functional π-Gelators and Their Applications, *Chem. Rev.*, 2014, **114**, 1973–2129.
27 S. Ghosh, V. K. Praveen and A. Ajayaghosh, The Chemistry and Applications of π-Gels, *Annu. Rev. Mater. Res.*, 2016, **46**, 235–262.
28 P. Terech and R. G. Weiss, Low Molecular Mass Gelators of Organic Liquids and the Properties of Their Gels, *Chem. Rev.*, 1997, **97**, 3133–3159.
29 D. J. Abdallah and R. G. Weiss, Organogels and Low Molecular Mass Organic Gelators, *Adv. Mater.*, 2000, **12**, 1237–1247.
30 X. Yan, F. Wang, B. Zheng and F. Huang, Stimuli-responsive supramolecular polymeric materials, *Chem. Soc. Rev.*, 2012, **41**, 6042–6065.
31 S. Panja and D. J. Adams, Stimuli responsive dynamic transformations in supramolecular gels, *Chem. Soc. Rev.*, 2021, **50**, 5165–5200.
32 K. Aoki, N. Tamaoki, A. Seki, K. Narazaki, D. Takahashi and K. Horitsugu, Synthesis and Properties of Aromatic-Terminated Diacetylene Organogelators and Their Application to Photopatterning of Polydiacetylenes, *Langmuir*, 2021, **37**, 13160–13169.
33 F. Xie, L. Qin and M. Liu, A dual thermal and photoswitchable shrinking–swelling supramolecular peptide dendron gel, *Chem. Commun.*, 2016, **52**, 930–933.
34 Q. Chen, Y. Feng, D. Zhang, G. Zhang, Q. Fan, S. Sun and D. Zhu, Light-Triggered Self-Assembly of a Spiropyran-Functionalized Dendron into Nano-/Micrometer-Sized Particles and Photoresponsive Organogel with Switchable Fluorescence, *Adv. Funct. Mater.*, 2010, **20**, 36–42.
35 S. Wang, W. Shen, Y. Feng and H. Tian, A multiple switching bisthienylethene and its photochromic fluorescent organogelator, *Chem. Commun.*, 2006, 1497–1499.
36 K. Kuroiwa, T. Shibata, A. Takada, N. Nemoto and N. Kimizuka, Heat-Set Gel-like Networks of Lipophilic Co(II) Triazole Complexes in Organic Media and Their Thermochromic Structural Transitions, *J. Am. Chem. Soc.*, 2004, **126**, 2016–2021.
37 J.-L. Pozzo, G. M. Clavier and J.-P. Desvergne, Rational design of new acid-sensitive organogelators, *J. Mater. Chem.*, 1998, **8**, 2575–2577.
38 S. A. Ahmed, X. Sallenave, F. Fages, G. Mieden-Gundert, W. M. Müller, U. Müller, F. Vögtle and J.-L. Pozzo, Multiaddressable Self-Assembling Organogelators Based on 2*H*-Chromene and *N*-Acyl-1,ω-amino Acid Units, *Langmuir*, 2002, **18**, 7096–7101.
39 S. R. Haines and R. G. Harrison, Novel resorcinarene-based pH-triggered gelator, *Chem. Commun.*, 2002, 2846–2847.
40 K. Sugiyasu, N. Fujita, M. Takeuchi, S. Yamada and S. Shinkai, Proton-sensitive fluorescent organogels, *Org. Biomol. Chem.*, 2003, **1**, 895–899.
41 F. Camerel, R. Ziessel, B. Donnio and D. Guillon, Engineering of an iron–terpyridine complex with supramolecular gels and mesomorphic properties, *New J. Chem.*, 2006, **30**, 135–139.

42 T. Becker, C. Y. Goh, F. Jones, M. J. McIldowie, M. Mocerino and M. I. Ogden, Proline-functionalised calix[4]arene: an anion-triggered hydrogelator, *Chem. Commun.*, 2008, 3900–3902.
43 Q. Jiang, H. Ruan, T. Wang, Y. Zhnag, Y. Qiu, H. Wang, Y. Liao and X. Xie, Extending Conjugation of Linear Cyanostilbene Derivatives via a Pyridine Moiety for Multi-Stimuli-Responsive Fluorescence Organogels, *Langmuir*, 2023, **39**, 10904–10912.
44 N. Sreenivasachary and J.-M. Lehn, Gelation-driven component selection in the generation of constitutional dynamic hydrogels based on guanine-quartet formation, *Proc. Natl. Acad. Sci. U. S. A.*, 2005, **102**, 5938–5943.
45 F. Lincker, A.-J. Attias, F. Mathevet, B. Heinrich, B. Donnio, J.-L. Fave, P. Rannoua and R. Demadrille, Influence of polymorphism on charge transport properties in isomers of fluorenone-based liquid crystalline semiconductors, *Chem. Commun.*, 2012, **48**, 3209–3211.
46 P. Sonar, T.-J. Ha and A. Dodabalapur, A fluorenone based low band gap solution processable copolymer for air stable and high mobility organic field effect transistors, *Chem. Commun.*, 2013, **49**, 1588–1590.
47 M. Shigeta, M. Morita and G. Konishi, Selective Formation of Twisted Intramolecular Charge Transfer and Excimer Emissions on 2,7-bis(4-Diethylaminophenyl)-fluorenone by Choice of Solvent, *Molecules*, 2012, **17**, 4452–4459.
48 J. Liu, L. Li, R. Xu, K. Zhang, M. Ouyang, W. Li, X. Lv and C. Zhang, Design, Synthesis, and Properties of Donor–Acceptor–Donor' Asymmetric Structured Electrochromic Polymers Based on Fluorenone as Acceptor Units, *ACS Appl. Polym. Mater.*, 2019, **1**, 1081–1087.
49 X. Pang, Y. Tan, C. Tan, W. Li, N. Du, Y. Lu and Y. Jiang, One-Step Construction of Fluorenone-Based Donor–Acceptor-Type Conjugated Polymers via Direct Arylation Polymerization for Cell-Imaging Applications, *ACS Appl. Mater. Interfaces*, 2019, **11**, 28246–28253.
50 Y. Zheng, P. Cheng, X. Qian, J. Guan, R. Shi, M. Xin, J. Xu and X.-H. Bu, Self-assembled organic nonlinear optical crystals based on pyridine derived fluorenone, *Mater. Chem. Front.*, 2023, **7**, 698–704.
51 M.-S. Yuan, D.-E. Wang, P. Xue, W. Wang, J.-C. Wang, Q. Tu, Z. Liu, Y. Liu, Y. Zhang and J. Wang, Fluorenone Organic Crystals: Two-Color Luminescence Switching and Reversible Phase Transformations between π–π Stacking-Directed Packing and Hydrogen Bond-Directed Packing, *Chem. Mater.*, 2014, **26**, 2467–2477.
52 K. Bader, C. Mueller, Y. Molard, A. Baro, P. Ehni, J. Knelles and S. Laschat, Fluorenone imidazolium salts as novel de Vries materials, *RSC Adv.*, 2020, **10**, 23999–24016.
53 K. Takatoh, K. Sunohara and M. Sakamoto, Mesophase Transition of Series Materials Containing Fluorene, Fluorenone and Biphenyl Structures with Chiral End Groups, *Mol. Cryst. Liq. Cryst.*, 1988, **164**, 167–178.
54 K. Takatoh and M. Sakamoto, Formation and Properties of Ferroelectric Liquid Crystalline Compound Containing –C(O)–S–O– Linkage, *Bull. Chem. Soc. Jpn.*, 1991, **64**, 2720–2723.
55 J. A. McCubbin, X. Tong, R. Wang, Y. Zhao, V. Snieckus and R. P. Lemieux, Directed Metalation Route to Ferroelectric Liquid Crystals with a Chiral Fluorenol Core: The Effect of Restricted Rotation on Polar Order, *J. Am. Chem. Soc.*, 2004, **126**, 1161–1167.
56 M. D. Harjung, C. P. J. Schubert, F. Knecht, J. H. Porada, R. P. Lemieux and F. Giesselmann, New amphiphilic materials showing the lyotropic analogue to the thermotropic smectic C* liquid crystal phase, *J. Mater. Chem. C*, 2017, **5**, 7452–7457.
57 H. Yoon, S.-W. Kang, M. Lehmann, J. O. Park, M. Srinivasarao and S. Kumar, Homogeneous and homeotropic alignment of bent-core uniaxial and biaxial nematic liquid crystals, *Soft Matter*, 2011, **7**, 8770–8775.
58 H. Su, R. Liu, M. Shu, M. Tang, J. Wang and H. Zhu, Fluorenone-based organogel and self-assembled fibrous film: Synthesis, optical properties and reversible detection of aniline vapor, *Dyes Pigm.*, 2019, **162**, 52–58.
59 K. Zhao, Y. Xiao, C. Guo, Q. Chang, H. Gao and X. Cheng, Control the self-assembly of fluorenone-based polycatenars by tuning chain length, *Tetrahedron*, 2019, **75**, 409–415.
60 H. Zhao and X. Cheng, Fluorene Thiophene α-Cyanostilbene Hexacatenar-Generating LCs with Hexagonal Columnar Phases and Gels with Helical Morphologies as Well as a Light-Emitting LC Display, *Int. J. Mol. Sci.*, 2023, **24**, 9337.
61 T. D. Thangadurai, C. J. Lee, S. H. Jeong, S. Yoon, Y. G. Seo and Y.-I. Lee, A novel colorimetric and fluorescent sensor for fluoride and pyrophosphate based on fluorenone signaling units, *Microchem. J.*, 2013, **106**, 27–33.
62 T. Chen, Z.-Q. Chen, W.-L. Gong, C. Li and M.-Q. Zhu, Ultrasensitive water sensors based on fluorenone-tetraphenylethene AIE luminogens, *Mater. Chem. Front.*, 2017, **1**, 1841–1846.
63 M. Mohar, 2,4,7-Triaminofluorenone as a Multi-Analyte Colorimetric Sensor of Fluoride, Acetone Vapor, and Other Harmful Compounds, *ChemistrySelect*, 2019, **4**, 8061–8067.
64 S. E. Thangaraj, E. J. Antony, G. T. Selvan, P. M. Selvakumar and I. V. M. V. Enoch, A New Fluorenone-based Turn-on Fluorescent Al^{3+} Ion Sensor, *J. Anal. Chem.*, 2019, **74**, 87–92.
65 J. Wang, Y. Cheng, J. Zhou and W. Tang, A donor–acceptor liganded metal–organic framework showcases the hydrogen-bond-enhanced sensing of N-heterocyclic explosives, *J. Mater. Chem. C*, 2021, **9**, 12086–12093.
66 H. M. Junaid, M. T. Waseem, Z. A. Khan, F. Munir, S. Sohail, U. Farooq and S. A. Shahzad, Fluorenone-Based Fluorescent and Colorimetric Sensors for Selective Detection of I^- Ions: Applications in HeLa Cell Imaging and Logic Gate, *ACS Omega*, 2022, **7**, 9730–9742.
67 N. Sharma and N. Kaur, Fluorenone Appended Colorimetric Sensor for Cascade Detection of Fluoride and Calcium Gluconate with Applications in Solid State and Logic Gate Systems, *ChemistrySelect*, 2023, **8**, e202204459.
68 S. Lv, X. Liu, H. Ding, X. Cheng, C. Yang, X. Xing, D. Qiu, X. Du and M.-S. Yuan, Unraveling the substituent group effects on the emission properties of fluorenone derivatives, *Dyes Pigm.*, 2023, **219**, 111619.

69 M. Brecl and T. Malavašič, Synthesis and Characterization of Side-Chain Liquid Crystal Polyurethanes, *J. Polym. Sci., Part A: Polym. Chem.*, 1997, **35**, 2871–2888.
70 N. Koumura, M. Kudo and N. Tamaoki, Photocontrolled Gel-to-Sol-to-Gel Phase Transitioning of meta-Substituted Azobenzene Bisurethanes through the Breaking and Reforming of Hydrogen Bonds, *Langmuir*, 2004, **20**, 9897–9900.
71 I. Yilgor, E. Yilgor, I. G. Guler, T. C. Ward and G. L. Wilkes, FTIR investigation of the influence of diisocyanate symmetry on the morphology development in model segmented polyurethanes, *Polymer*, 2006, **47**, 4105–4114.
72 X. Lu, Y. Wang and X. Wu, Study of hydrogen bonds in polyester-polyurethanes by solution n.m.r, *Polymer*, 1994, **35**, 2315–2320.
73 K. E. Rowe and D. W. Bruce, The synthesis and mesomorphism of di-, tetra- and hexa-catenar liquid crystals based on 2,2′-bipyridine, *J. Mater. Chem.*, 1998, **8**, 331–341.
74 T. Yasuda, H. Ooi, J. Morita, Y. Akama, K. Minoura, M. Funahashi, T. Shimomura and T. Kato, π-Conjugated Oligothiophene-Based Polycatenar Liquid Crystals: Self-Organization and Photoconductive, Luminescent, and Redox Properties, *Adv. Funct. Mater.*, 2009, **19**, 411–419.
75 C. Cuerva, J. A. Campo, P. Ovejero, M. R. Torres and M. Cano, Polycatenar pyrazole and pyrazolate ligands as building blocks of new columnar Pd(II) metallomesogens, *Dalton Trans.*, 2014, **43**, 8849–8860.
76 M. J. Frisch, G. W. Trucks, H. B. Schlegel, G. E. Scuseria, M. A. Robb, J. R. Cheeseman, G. Scalmani, V. Barone, B. Mennucci, G. A. Petersson, H. Nakatsuji, M. Caricato, X. Li, H. P. Hratchian, A. F. Izmaylov, J. Bloino, G. Zheng, J. L. Sonnenberg, M. Hada, M. Ehara, K. Toyota, R. Fukuda, J. Hasegawa, M. Ishida, T. Nakajima, Y. Honda, O. Kitao, H. Nakai, T. Vreven, J. A. Montgomery, Jr., J. E. Peralta, F. Ogliaro, M. Bearpark, J. J. Heyd, E. Brothers, K. N. Kudin, V. N. Staroverov, R. Kobayashi, J. Normand, K. Raghavachari, A. Rendell, J. C. Burant, S. S. Iyengar, J. Tomasi, M. Cossi, N. Rega, J. M. Millam, M. Klene, J. E. Knox, J. B. Cross, V. Bakken, C. Adamo, J. Jaramillo, R. Gomperts, R. E. Stratmann, O. Yazyev, A. J. Austin, R. Cammi, C. Pomelli, J. W. Ochterski, R. L. Martin, K. Morokuma, V. G. Zakrzewski, G. A. Voth, P. Salvador, J. J. Dannenberg, S. Dapprich, A. D. Daniels, Ö. Farkas, J. B. Foresman, J. V. Ortiz, J. Cioslowski and D. J. Fox, *Gaussian 09, Revision D.01*, Gaussian, Inc., Wallingford CT, 2009.
77 C. Lee, W. Yang and R. G. Parr, Development of the Colle-Salvetti correlation-energy formula into a functional of the electron density, *Phys. Rev. B: Condens. Matter Mater. Phys.*, 1988, **37**, 785–789.
78 A. D. Becke, Density-functional thermochemistry. III. The role of exact exchange, *J. Chem. Phys.*, 1993, **98**, 5648–5652.
79 G. A. Petersson, A. Bennett, T. G. Tensfeldt, M. A. Al-Laham, W. A. Shirley and J. Mantzaris, A complete basis set model chemistry. I. The total energies of closed-shell atoms and hydrides of the first-row elements, *J. Chem. Phys.*, 1988, **89**, 2193–2218.
80 G. A. Petersson and M. A. Al-Laham, A complete basis set model chemistry. II. Open-shell systems and the total energies of the first-row atoms, *J. Chem. Phys.*, 1991, **94**, 6081–6090.
81 A. S. Klymchenko and A. P. Demchenko, Multiparametric probing of intermolecular interactions with fluorescent dye exhibiting excited state intramolecular proton transfer, *Phys. Chem. Chem. Phys.*, 2003, **5**, 461–468.
82 M. H. Abraham, Hydrogen bonding. 31. Construction of a scale of solute effective or summation hydrogen-bond basicity, *J. Phys. Org. Chem.*, 1993, **6**, 660–684.
83 M. H. Abraham, H. S. Chadha, G. S. Whiting and R. C. Mitchell, Hydrogen Bonding. 32. An Analysis of Water-Octanol and Water-Alkane Partitioning and the Δlog *P* Parameter of Seiler, *J. Pharmacol. Sci.*, 1994, **83**, 1085–1100.
84 A. S. Klymchenko and A. P. Demchenko, Electrochromic Modulation of Excited-State Intramolecular Proton Transfer: The New Principle in Design of Fluorescence Sensors, *J. Am. Chem. Soc.*, 2002, **124**, 12372–12379.
85 A. S. Klymchenko, T. Ozturk and A. P. Demchenko, Synthesis of furanochromones: a new step in improvement of fluorescence properties, *Tetrahedron Lett.*, 2002, **43**, 7079–7082.